Microchimica Acta (2020) 187:609
https://doi.org/10.1007/s00604-020-04588-x

ORIGINAL PAPER

Electrochemical synthesis and characterization of poly(thionine) -deep eutectic solvent/carbon nanotube–modified electrodes and application to electrochemical sensing

Berna Dalkıran[1] · Isabel P. G. Fernandes[1] · Melinda David[1] · Christopher M. A. Brett[1]

Received: 27 May 2020 / Accepted: 1 October 2020
© Springer-Verlag GmbH Austria, part of Springer Nature 2020

Abstract

Electropolymerization of thionine (TH) on multiwalled carbon nanotube (MWCNT)–modified glassy carbon electrodes (GCE) in ethaline deep eutectic solvent (DES) was carried out for the first time, to prepare poly(thionine) (PTH) films with different nanostructured morphologies. PTH films were formed on MWCNT/GCE by potential cycling electropolymerization in ethaline with the addition of different acid dopants CH_3COOH, $HClO_4$, HNO_3, H_2SO_4 and HCl, acetic acid being the best. The electropolymerization process was monitored with an electrochemical quartz crystal microbalance. The polymerization scan rate was a key factor affecting the electrochemical and morphological properties of the $PTH_{Ethaline}$-CH_3COOH/MWCNT/GCE; electrodeposition at 200 mV s^{-1} showing the best performance. The PTH/MWCNT/GCE platform was characterized using cyclic and differential pulse voltammetry, electrochemical impedance spectroscopy and scanning electron microscopy. The analytical characteristics of the PTH films were evaluated for sensing of ascorbic acid and biosensing of uric acid. The developed sensor exhibited a low detection limit (1.1 μM), wide linear range (2.8–3010 μM) and high sensitivity (1134 μA cm^{-2} mM^{-1}) for ascorbic acid. After immobilization of uricase, UOx, on PTH/MWCNT/GCE, the biosensor was successfully applied to the determination of uric acid, with fast response (< 7 s), good sensitivity (450 μA cm^{-2} mM^{-1}, wide linear range (0.48–279 μM) and low detection limit (58.9 nM), better than in the literature and than with PTH prepared in aqueous solution. The determination of uric acid in synthetic urine samples was successfully tested and the mean analytical recovery was 100.8 ± 1.4%. This is a promising approach for the determination of uric acid in real samples.

Keywords Ethaline deep eutectic solvent · Electropolymerization · Poly(thionine) · Carbon nanotubes · Biosensor · Uric acid

Introduction

Applications of electrochemical sensors and biosensors depend on the sensing materials on the electrode surfaces and their nanostructure, addressing important challenges such as fast response, high sensitivity and selectivity with low detection limits and enhancing electrocatalytic effects. Many new sensor platforms are based on carbon electrodes coated with carbon nanomaterials, often used to immobilize biomolecules, and have been used in healthcare, food and environmental applications due to important properties such as low cost, high conductivity and fast electron transfer rates [1, 2]. Such carbon nanomaterials are exemplified by carbon nanotubes (CNT), graphene and carbon black [3, 4]. CNT have been widely explored for such purposes, due to their electrical, chemical, mechanical and structural properties [5], as well as promoting electron transfer reactions [6].

This work focuses on the development of a new sensor platform based on glassy carbon electrodes (GCE) using functionalized multiwall carbon nanotubes (MWCNT), and electroactive polymers. The use of electroactive polymers together with MWCNT is advantageous because it combines the electrical conductivity and mechanical strength of the polymer-carbon nanomaterial matrices with enhanced analytical performance [5]. The general purpose is to explore the uses of such sensor architectures and compare them with platforms that use other nanomaterials such as metal or metal oxide nanoparticles.

Electronic supplementary material The online version of this article (https://doi.org/10.1007/s00604-020-04588-x) contains supplementary material, which is available to authorized users.

✉ Christopher M. A. Brett
cbrett@ci.uc.pt

[1] CEMMPRE, Department of Chemistry, University of Coimbra, 3004-535 Coimbra, Portugal

Published online: 15 October 2020

The use of deep eutectic solvents (DES), green solvents employed as an alternative to conventional solvents and ionic liquids, in the synthesis of electroactive polymers has led to polymers with higher electronic conductivity compared to those obtained in aqueous media [7]. DES have important advantages of low cost, low toxicity, biocompatibility, good conductivity and chemical stability, and a wide electrochemical window. They also have a huge potential as electrolytic media for the electrodeposition of metals and polymers, which make them important for biosensor applications [8]. The physicochemical properties of DES can be tuned, depending on the two components, the hydrogen bond acceptor and the hydrogen bond donor, which, mixed in the correct molar fractions, lead to the eutectic mixture [9]. Pure DES by itself often has a relatively low conductivity, that can limit the rate of some processes such as the electrodeposition of polymers. Additives such as acids, salts and amine derivatives can increase the conductivity and change the properties of the electrodeposited material in terms of its conductivity, redox behaviour and dopant incorporation [7, 10].

The present work concerns the preparation, characterization and application of GCE coated with MWCNT on top of which a film of the electroactive polymer poly(thionine) (PTH) is formed by potential cycling electropolymerization in acid-doped ethaline DES under different experimental conditions. The deposition process was studied with the electrochemical quartz crystal microbalance (EQCM). The modified electrode with the best architecture was electrochemically characterized by cyclic voltammetry (CV), differential pulse voltammetry (DPV) and electrochemical impedance spectroscopy (EIS). Scanning electron microscopy (SEM) was used to examine the morphology of the PTH films, and correlated with the electrochemical behaviour.

The applicability of PTH-modified electrodes prepared in DES was demonstrated by sensing ascorbic acid (AA). Biosensing application was illustrated by immobilizing the enzyme uricase (UOx), using the platform for the detection of uric acid (UA), the final product of purine metabolism in blood and urine. Physiological levels of UA in human plasma and urine are normally between 2.5 and 6 mg/100 mL (0.15–0.36 mM), while those of AA are 0.6 and 1.5 mg/100 mL (0.034–0.085 mM) [11]. Compared with these species, the concentration of dopamine in biological fluids is very low (in the range of several tens of nanomolar) [12]. Abnormal UA levels in the human body can cause a number of diseases, including hyperuricemia, gout and anemia [13].

Experimental

Reagents and solutions

All reagents and solvents were of analytical grade and were used without further purification. Uricase from BioChemika (UOx, 94310, from *Bacillus fastidious*, 16.2 U/mg), uric acid, L-ascorbic acid, dopamine hydrochloride, NaCl, $MgCl_2.6H_2O$, urea, thionine, choline chloride, chitosan from crab shells, ethylene glycol, sulphuric acid, nitric acid, acetic acid, phosphoric acid and glutaraldehyde (25% *v*/v in water) were purchased from Sigma-Aldrich, Germany. Boric acid was from JT Baker, Netherlands. $NaH_2PO_4.H_2O$, H_2PO_3, KH_2PO_4, α-D-glucose, perchloric acid and hydrochloric acid were obtained from Riedel-de-Haën, Germany, and $Na_2HPO_4.2H_2O$ from Fluka, Switzerland. Na_2SO_4, NH_4Cl and creatinine were purchased from Merck, Switzerland. KCl was supplied by PanReac, Spain. MWCNT, outer diameter 30 ± 10 nm, were from NanoLab, USA.

Britton-Robinson buffer (BR) was used as supporting electrolyte and was prepared by mixing phosphoric acid, boric acid and acetic acid (all at 0.040 M) and adjusting the pH with 1 M NaOH. The 0.1 M phosphate buffer (PB, pH = 7.0) was prepared by mixing $NaH_2PO_4.H_2O$ and $Na_2HPO_4.2H_2O$ in the appropriate proportions and was used as supporting electrolyte for biosensor evaluation.

A synthetic urine sample was preparing a solution in water containing the following components [14]: 6 mM $MgCl_2$, 50 mM NaCl, 21 mM KCl, 16 mM Na_2SO_4, 20 mM KH_2PO_4, 18 mM NH_4Cl, 416 mM urea, 9 mM creatinine and 9.5 mM uric acid. The mixture was sonicated to obtain a homogeneous solution and then adjusted to pH 6.0 with 1 M NaOH and HCl.

All aqueous solutions were prepared with deionized water (Millipore Milli-Q Ultrapure Water System). All experiments were carried out at room temperature (25 ± 1 °C).

Apparatus and measurements

Voltammetric experiments were carried out using an Ivium CompactStat electrochemical analyzer (Ivium Technologies, Netherlands). A conventional three-electrode cell was equipped with a modified GCE (geometric area 0.00785 cm^2) as working electrode, an Ag/AgCl electrode (3 M KCl) as reference and a platinum wire as counter electrode. Gravimetric studies were performed with an electrochemical quartz crystal microbalance (EQCM 10M, Gamry Instruments) containing a gold quartz crystal (AuQC) with 10 MHz central frequency. Electrochemical impedance measurements were performed with a Solartron 1250 Frequency Response Analyzer coupled to a Solartron 1286 Electrochemical Interface using ZPlot 2.4 software (Solartron Analytical, UK). A sinusoidal voltage perturbation of amplitude 10 mV rms was applied in the frequency range between 65 kHz and 0.1 Hz with 10 frequency steps per decade. Scanning electron microscopy (SEM) (JEOL, JSM-5310, Japan) was used to characterize the surface morphology of the nanostructured nanocomposites on carbon film electrodes. The pH measurements were made with a CRISON 2001 micropH-meter (Crison Instruments SA, Spain) at room temperature.

Pre-treatment of GCE and modification by carbon nanotubes

The bare GCE surface was polished before each experiment or modification with 1 μm particle size diamond spray (Kemet, UK), rinsed with Milli-Q water and then placed in an ultrasonic bath for 10 min in ethanol. Activation of the GCE is necessary to ensure the reproducibility of experimental results. For this purpose, the GCE was placed in 0.1 M PB containing 0.1 M KCl and cyclic voltammograms (CVs) were recorded between the potential limits of − 0.6 and + 0.9 V until a steady-state baseline voltammogram was obtained, generally 5 cycles.

Acidic functionalization of MWCNT was done in 3 M HNO_3 and is described in previous work [15]. The MWCNTs were then dispersed in a chitosan solution (1% *w*/*v* chitosan in 1% *v*/*v* acetic acid) and sonicated for 3 h. The amount of MWCNT present in the suspension was 1%. A volume of 1 μL of the suspension was dropped on the GCE surface and allowed to dry at room temperature. After complete drying, the procedure was repeated once more.

Preparation of ethaline- and poly(thionine)-modified electrodes

Amongst the many DES in the literature [16], ethaline was chosen, since previous work showed that it is a good choice for polymer formation by electropolymerization [10]. Ethaline results from interaction between the hydrogen acceptor choline chloride (ChCl) and the hydrogen bond donor ethylene glycol (EG), the eutectic mixture corresponding to a molar ratio of 1:2. Solid ChCl is first heated up to ~ 100 °C to evaporate any water. Then, EG is added, and the mixture is held at a constant temperature of ~ 60 °C, while continuously stirring, until homogenization occurs. The ethaline is then cooled down to room temperature and is ready for use.

Different amounts of TH were dissolved in ethaline DES under constant stirring, heating the solution slightly to 30–40 °C in order to facilitate homogenization. A small quantity of acid (CH_3COOH, $HClO_4$, HNO_3, H_2SO_4 or HCl) with final concentration 1 M was added to increase the amount of ionic species in the viscous mixture, enabling a higher rate of diffusion and slightly reducing the viscosity. The best concentration of monomer was found to be 1 mM.

Films of PTH were formed by electropolymerization on MWCNT/GCE using potential cycling, the optimized scan rate being 200 mV s^{-1}, during 15 scans. The potential was cycled in the potential range − 0.5 to + 0.8 V vs. Ag/AgCl. For comparison, PTH film–coated electrodes were formed in aqueous solution containing 1.0 mM TH + 0.025 M $Na_2B_4O_7$ + 0.10 M KNO_3. Characterization of PTH films was performed in Britton-Robinson (BR) buffer solution pH = 7.0, by CV in the potential range − 0.5 to + 0.5 V vs. Ag/AgCl, at a scan rate of 100 mV s^{-1}.

Biosensor preparation

For biosensor preparation, uricase (UOx) was immobilized on $PTH_{Ethaline}$-CH_3COOH/MWCNT/GCE. An UOx solution, concentration of 5 mg/mL, was prepared in 0.1 M PB (pH = 7.0). A volume of 2 μL of the prepared enzyme solution was dropped onto the PTH_{DES}-modified MWCNT/GCE surface together with 1 μL of glutaraldehyde (2.5%) and left to dry before being used for the determination of uric acid. When the biosensor was not in use, it was stored at 4 °C in 0.1 M PB solution.

Results and discussion

Electropolymerization of thionine

The electropolymerization parameters such as the electrolyte composition, pH, monomer concentration, number of potential cycles and scan rate are important for the growth and final properties of the polymer film [15–17].

The influence of TH monomer concentration was tested with different concentrations between 0.5 and 2.0 mM. To investigate the influence of electrolyte, ethaline DES containing different dopant acids (CH_3COOH, $HClO_4$, HNO_3, H_2SO_4 and HCl) were prepared (text and Fig. S1 in Supplementary Information). The best result for the polymer film growth was obtained at a monomer concentration of 1.0 mM TH in CH_3COOH-doped DES (Fig. 1); above this the polymer growth rate showed a very slight decrease. This could be due to the formation of a thick and non-uniform film at high monomer concentrations with a higher nucleation rate and lower adherence [18]. PTH is an electroactive polymer with heterocyclic nitrogen atoms, nitrogen bridges and free amino groups. The polymerization mechanism of TH can be explained by the fact that when the polymer film is formed, free amine groups turn into nitrogen bridges and these bridges become electroactive [19, 20]. The interaction between PTH and MWCNT on the growth of the polymer has also been studied [21, 22]. For TH polymerization, strong electrostatic interactions between MWCNT and PTH can be attributed to the negatively charged functionalized MWCNT, interacting with the positively charged sulphur of PTH [15, 21].

In Fig. 1, it can be seen that the CVs for forming $PTH_{Ethaline}$-CH_3COOH/MWCNT/GCE contain two oxidation and two reduction peaks. One redox couple can correspond to entrapped monomer oxidation/reduction (II_a/II_c) and the other to polymer oxidation/reduction (I_a/I_c); the current response increases with the number of cycles showing the growth of the PTH film [22].

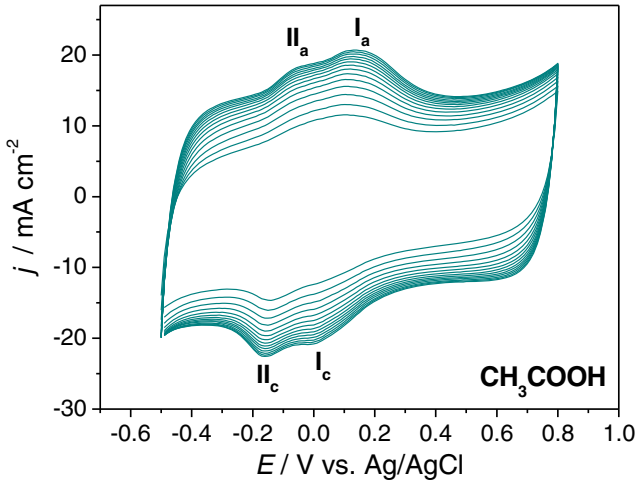

Fig. 1 Potential cycling electropolymerization of TH from a solution of 1 mM TH in ethaline with 1.0 M CH_3COOH on MWCNT/GCE at scan rate 200 mV s^{-1}

The influence of scan rate on the electropolymerization of TH was examined in the optimized DES solution composition. CV curves during the growth of the $PTH_{Ethaline}$-CH_3COOH film on the MWCNT/GCE surface in DES during 15 cycles were recorded at different scan rates from 100 to 300 mV s^{-1} (Supplementary Information Fig. S2A-D). The peak currents for PTH increased with increasing scan rate up to 200 mV s^{-1}, showing successful diffusional transport of the monomer from solution to the MWCNT/GCE surface [18]. At higher scan rates, the polymer growth rate decreases owing to diffusion limitations in the viscous medium [15, 18, 23]. The CV curves in Fig. S2E, of the PTH-modified electrodes, recorded in 0.1 M BR buffer (pH 7.0) at a scan rate of 100 mV s^{-1} lead to the same conclusion that $PTH_{DES}200$ is the best architecture.

Electrochemical quartz crystal microbalance

EQCM was used to monitor the dynamics of the adsorption of TH and the electropolymerization process on gold quartz crystals. The frequency variation with time can be used both for film growth monitoring and also for evaluating the influence of anion sources which are incorporated or expelled from PTH film during the potential cycling polymerization process. For $PTH_{Ethaline}$-CH_3COOH film formation, cycling was done between −0.5 and +0.8 V vs. Ag/AgCl, at a scan rate of 200 mV s^{-1} for 15 cycles. Figure 2a shows the change of frequency as a function of time. The variation of frequency can be used to determine the deposited mass assuming a rigid film, using the Sauerbrey equation, as in [18]. The mass/frequency correlation factor of the gold-coated quartz crystal employed in this study is 226.0 Hz per 1 μg.

On examining Fig. 2a, it is seen that the frequency does not decrease upon mass uptake which suggests that the Sauerbrey equation for rigid films does not apply. The microbalance used in this work permits the simultaneous recording of two resonant frequencies, in series (f_s) and in parallel (f_p), as shown in Fig. 2b. The dissimilarity between the two frequencies indicates the formation of a non-rigid film, which has been previously seen for film formation in DES media [10]. In such cases, the change in frequency also depends upon the viscosity and density of the solution; coupling of a viscous solution to the oscillating crystal surface results in a change in the series resonant frequency and damping of the resonant oscillation [24].

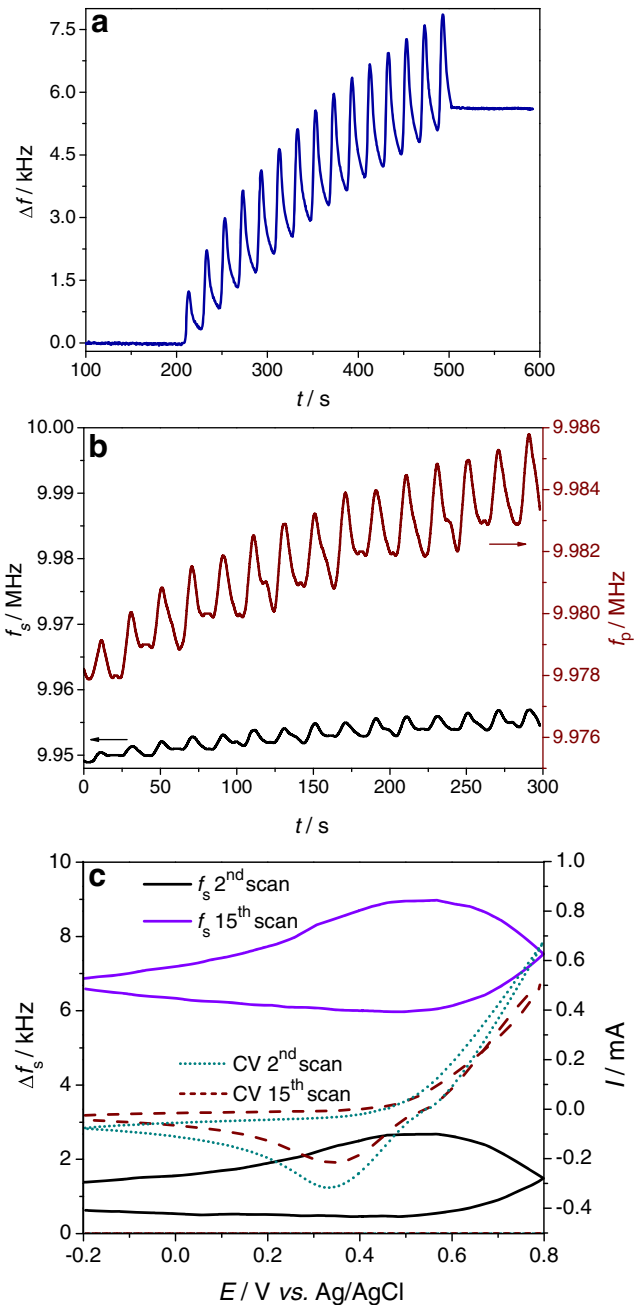

Fig. 2 **a** EQCM measurements monitored at an AuQC for PTH film formation in ethaline DES. **b** EQCM response in terms of series resonant frequency (f_s) and parallel-resonant frequency (f_p) with time for PTH_{DES} film formation. **c** CV and massogram during PTH_{DES} film formation for the 2nd and 15th cycle

To further analyze this perspective and since ethaline is a viscous medium, we assume that a viscoelastic film will form on the AuQC during polymerization. The behaviour of viscoelastic films is complex, depending on the mechanical properties of the materials, the shear wavelength and film thickness. For a low value of the shear modulus, friction within a viscous film will appear and lead to dissipation. Since electromechanical coupling occurs in the QC, the properties of the liquid media will be reflected in the electrical properties of the resonator: the resistance decreases as the film viscosity increases [25].

To detect the changes in viscoelastic properties of a redox film, the simultaneous monitoring of the series resonance resistance during electropolymerization is recommended [26], as shown in Fig. 2c. The frequency-potential diagram shows a frequency increase from the 2nd to the 15th cycle, but when analyzing each cycle separately, since the potential is scanned in a positive direction, upon reduction of PTH, a frequency decrease can be noticed. This decrease is more pronounced for the first 5 cycles (only the 2nd cycle is illustrated) compared with the following 10 polymerization cycles. This is also in agreement with the more pronounced PTH film formation during the first 5 cycles of electropolymerization, where the reduction peak at 0.35 V keeps increasing.

Electrochemical characterization of $PTH_{Ethaline}$-CH_3COOH/MWCNT/GCE

Influence of pH

Due to the amino groups of PTH, the electrochemical behaviour of PTH is highly dependent on pH [27]. The influence of the pH value on the electrochemical profile of $PTH_{Ethaline}$-CH_3COOH/MWCNT/GCE, redox couple I, was evaluated by DPV. The DPV measurements were made with a pulse amplitude of 10 mV, a step potential of 2 mV and a scan rate of 50 mV s^{-1} in 0.1 M BR buffer solution at different values of pH. In Fig. 3a, it can be seen that when the pH value is increased from 2.0 to 8.0 in BR buffer solution, the anodic peak potential (E_{pa}) shifts negatively with a linear dependence on pH. The equation for variation of peak potential with pH was $E_{pa} = 0.0286–0.030$ pH, with a slope of 30 mV pH^{-1}, see Fig. S3A, meaning that the number of protons is half the number of electrons participating in the oxidation process. The value of the peak half-width ($W_{1/2} \approx 80$ mV) suggests that the total number of electrons is equal to 2, so the process involves 2 electrons and 1 proton. The highest peak current was obtained at pH 7.0. Hence, pH 7.0 was considered to be the best pH for further experiments.

Influence of scan rate

CVs at $PTH_{Ethaline}$-CH_3COOH/MWCNT/GCE in 0.1 M BR (pH 7.0) were recorded at scan rates ranging from 10 to 100 mV s^{-1}, Fig. 3b, to examine the influence of scan rate on the electrochemical behaviour of the modified electrode. Fig. S3B shows that both the anodic and the cathodic peak currents increase linearly with scan rate (10–100 mV s^{-1}), implying a surface controlled electrochemical mechanism [21, 28]. In all cases, two redox couples were observed, for the redox couple (I_a/I_c) $j_{pIa} = 0.05\ v - 0.43$ and $j_{pIc} = 0.05\ v + 0.21$, and for the redox couple (II_a/II_c) $j_{pIIa} = 0.06\ v - 0.12$ and $j_{pIIc} = 0.07\ v - 0.15$.

Moreover, linear relationships were obtained between log (j_p) and log (v) with the slopes of 0.99 and 0.98 for j_{pa} and 0.98 and 0.98 for j_{pc}. The ratio of j_{pa}/j_{pc} is close to the theoretical value of 1.0, confirming that the redox mechanism of PTH is adsorption controlled, in agreement with literature reports [19].

Electrochemical impedance spectroscopy

EIS was used to characterize the $PTH_{Ethaline}$-CH_3COOH/MWCNT/GCE with PTH films electrodeposited at different scan rates. For this purpose, impedance spectra of the $PTH_{Ethaline}$-CH_3COOH/MWCNT/GCE were obtained in 0.1 M BR buffer solution (pH = 7.0) at − 0.1 V vs. Ag/AgCl. The applied potential was chosen from the CV of $PTH_{ethaline}$-CH_3CHOOH on the MWCNT/GCE surface in BR buffer at 200 mV s^{-1} in Fig. S2E.

Complex plane impedance spectra are shown in Fig. 4a and all consist of three parts, a semicircle in the high-frequency region and two linear regions. All spectra were fitted to the same electrical equivalent circuit (Fig. 4b). R_Ω is the cell resistance which is followed by a semicircle in the high-frequency region, that can be attributed to the interfacial region between the electrode substrate and the polymer film/MWCNT comprising a charge transfer resistance in parallel with charge separation, modelled by the parallel RC combination R_1C_1. The linear part at medium frequency is attributed to diffusion through the modifier film and is represented by a Warburg-type impedance according to $Z_W = R_D\mathrm{cth}[(\tau i\omega)^{\alpha}](\tau i\omega)^{-\alpha}$, where $\alpha < 0.5$, with R_D the diffusional resistance, and τ the diffusional time constant. The CPE, at low frequency, is expressed as a non-ideal capacitance of the modifier film-solution interface with $\mathrm{CPE} = [(Ci\omega)^{\alpha}]^{-1}$; there are no faradaic processes under the experimental conditions employed. The values of the CPE exponents (α) can vary between 0.5 and 1.0 corresponding to porous and to completely uniform and smooth electrode surfaces, respectively [21].

The parameter values obtained by fitting the spectra for $PTH_{Ethaline}$-CH_3COOH/MWCNT/GCE prepared at different scan rates from 100 to 300 mV s^{-1} are summarized in Table S1 (Supplementary Information). The fitting values close to the value of 1.0 show that the modified electrodes have a relatively uniform and smooth surface at the molecular and nanometric level. It can be seen that an increase in the

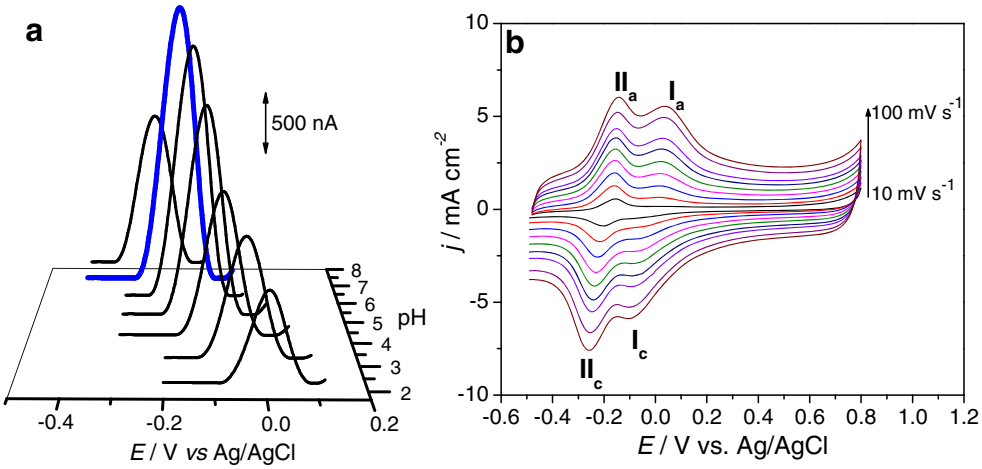

Fig. 3 **a** Differential pulse voltammograms for the oxidation of $PTH_{Ethaline}$-CH_3COOH/MWCNT/GCE in 0.1 M BR buffer solution at pH 2.0 to 8.0. The thicker voltammogram in blue for pH 7.0 has the highest peak current. **b** CVs of $PTH_{Ethaline}$-CH_3COOH/MWCNT/GCE in 0.1 M BR buffer solution (pH 7.0) at scan rates from 10 to 100 mV s^{-1}

scan rate during synthesis leads to a decrease in R_1 values and an increase in the C_1 values in Table S1. The R_1 value refers to the interface between the polymer film and the GCE, a decrease in R_1 indicating easier charge transfer between the electrode and polymer film [29].

The values of R_1 are in the order: PTH_{DES}-300 > PTH_{DES}-100 > PTH_{DES}-150 > PTH_{DES}-200. This indicates that an increased scan rate can contribute to facilitating electron transfer, probably due to a greater area of physical contact up to 200 mV s^{-1} scan rate. However, the R_1 value decreases above 200 mV s^{-1}, which can be attributed to the decrease in species able to access the electrode surface due to the ethaline viscosity beginning to have an influence [30]. In addition, for all polymer-modified electrodes, the decrease in R_1 values is accompanied by an increase in C_1. The fastest interfacial charge transfer occurs at the electrode configuration PTH_{DES}-200, in agreement with the CV in Fig. S2.

In relation to the diffusion impedance, the α values are more or less constant and close to what would be obtained for a film with no non-uniform effects. The values of Z_W are similar except for 300 mV s^{-1} films, which suggests that the film has different characteristics and is possibly internally more porous. Finally, the large values of the CPE show a relatively smooth interface at the molecular/nanometric scale (exponent ~ 0.95 in all cases) and a large capacitance of what is exposed to solution, to be expected owing to the existence of the CNT.

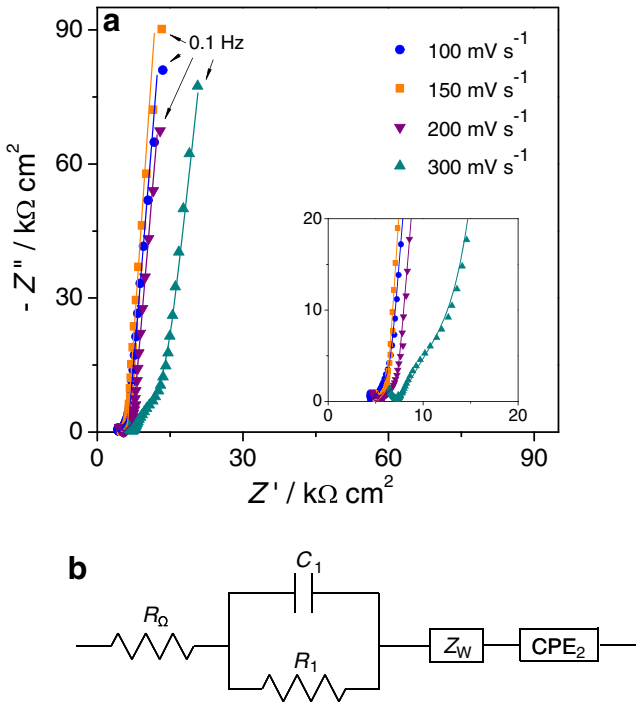

Fig. 4 **a** Complex plane impedance spectra of $PTH_{Ethaline}$-CH_3COOH/MWCNT/GCE in 0.1 M BR buffer solution (pH = 7.0) at − 0.1 V vs. Ag/AgCl for different polymerization scan rates. **b** The electrical equivalent circuit used to fit the spectra

Surface morphological characterization

Morphological characterization of MWCNT and of PTH films prepared at different scan rates (100, 150, 200 and 300 mV s^{-1}) on MWCNT surfaces was done by scanning electron microscopy on carbon film electrode supports. As seen in the inset of Fig. 5a, the MWCNT are uniformly embedded in the chitosan matrix, and show that it is suitable as substrate for the polymerization of TH due to its highly porous and regular surface morphology [21]. Images of PTH_{DES} films as a function of the polymerization scan rate are shown in Fig. 5a–d. The morphology of the PTH_{DES}-100 in Fig. 5a shows thin film formation on the MWCNT surface and this caused only minor changes in the size of the MWCNT. For scan rates higher than 100 mV s^{-1}, the polymer film formed is thicker. PTH_{DES}-200 nanocomposite film (Fig. 5c) appears more uniform and smoother than PTH_{DES}-150 and PTH_{DES}-300. As shown in Fig. 5b, PTH_{DES}-150 film has high roughness wit evidence of some remaining porosity. Although the film formed at a higher scan rate of 300 mV s^{-1} has a relatively non-porous surface, it shows poorer electrochemical behaviour than the PTH_{DES}-200 (see the

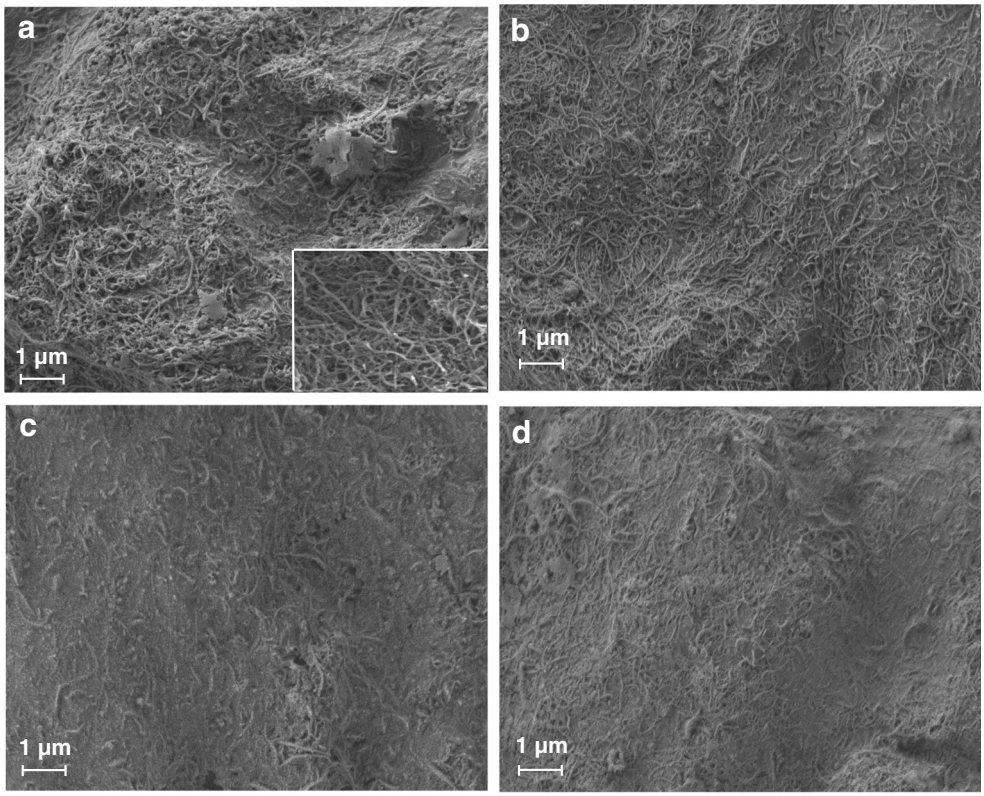

Fig. 5 SEM images on carbon film electrode (CFE) supports of **a** $PTH_{DES}100$/MWCNT, **b** $PTH_{DES}150$/MWCNT, **c** $PTH_{DES}200$/MWCNT and **d** $PTH_{DES}300$/MWCNT (EHT = 2.0 kV; Mag = × 10.000). The inset in **a** shows MWCNT on the CFE

"Electropolymerization of thionine" and "Electrochemical characterization of $PTH_{Ethaline}$-CH_3COOH/MWCNT/GCE" sections).

It is expected that the scan rate has an effect on the formation and the growth of electrochemically deposited PTH, because polymer nuclei have a crucial role in controlling the diameter of carbon nanotubes [31]. At slower scan rates, the formation of poly(thionine) nuclei, which cause rapid growth of the polymer, slows down, and a thinner and non-porous structure is formed. In contrast, when the scan rate increases, the time spent for the deposition of PTH becomes smaller, which causes the growth rate of the film decreases and the structure is more compact [32].

Analytical determination of ascorbic acid and uric acid

To illustrate potential applications, the analytical characteristics of $PTH_{Ethaline}$-CH_3COOH/MWCNT/GCE for the determination of AA and UA were evaluated.

Ascorbic acid

The amperometric detection of the model analyte AA by fixed potential chronoamperometry was carried out using the MWCNT/GCE modified by different PTH films obtained in DES at scan rates from 100 to 300 mV s^{-1}. To investigate the influence of the applied potential on sensor response, the CVs of the sensor in 0.1 M PB solution in the absence and presence of the AA species were examined. The maximum peak currents for AA oxidation in CVs were obtained at 0.0 V. Figure 6A1 shows a typical steady-state amperometric response and Fig 6A2 the calibration curves of sensors at $PTH_{Ethaline}$-CH_3COOH/MWCNT/GCE for the successive addition of AA. In Fig. 6A2, comparing the calibration plots, it is clearly seen that the highest sensitivity for the determination of AA was obtained with $PTH_{DES}200$-modified MWCNT/GCE. The calibration curve of the $PTH_{DES}200$ sensor was found to have a linear range of 2.8–3010 μM with a sensitivity of 1134 μA cm^{-2} mM^{-1} (8.90 μA mM^{-1}) for ascorbic acid. The LOD of the biosensor was found to be 1 μM for $PTH_{Ethaline}200$-CH_3COOH/MWCNT/GCE, following the linear equation: Δj (μA cm^{-2}) = − 1.03 + 2.45 × 10^{-3} [Ascorbic Acid] (μM), with a correlation coefficient (R^2) equal to 0.9987. Thus, the $PTH_{DES}200$ seems the most appropriate for sensor application.

The linear range and detection limit of the sensor for AA (2.8–3010 μM and 1.1 μM) are much better than those of other studies in recent years. Habibi et al. [33], developed an enhanced MWCNT-modified carbon-ceramic sensor with a LOD of 7.71 μM in the range of 15–800 μM. An AA sensor based on nitrogen-doped graphene showed a linear range of 5–1300 μM and detection limit of 2.22 μM [34]. Luo et al. [35] with a polyaniline/poly(styrenesulfonic acid)–modified graphene composite electrode found an LOD of 5 μM and

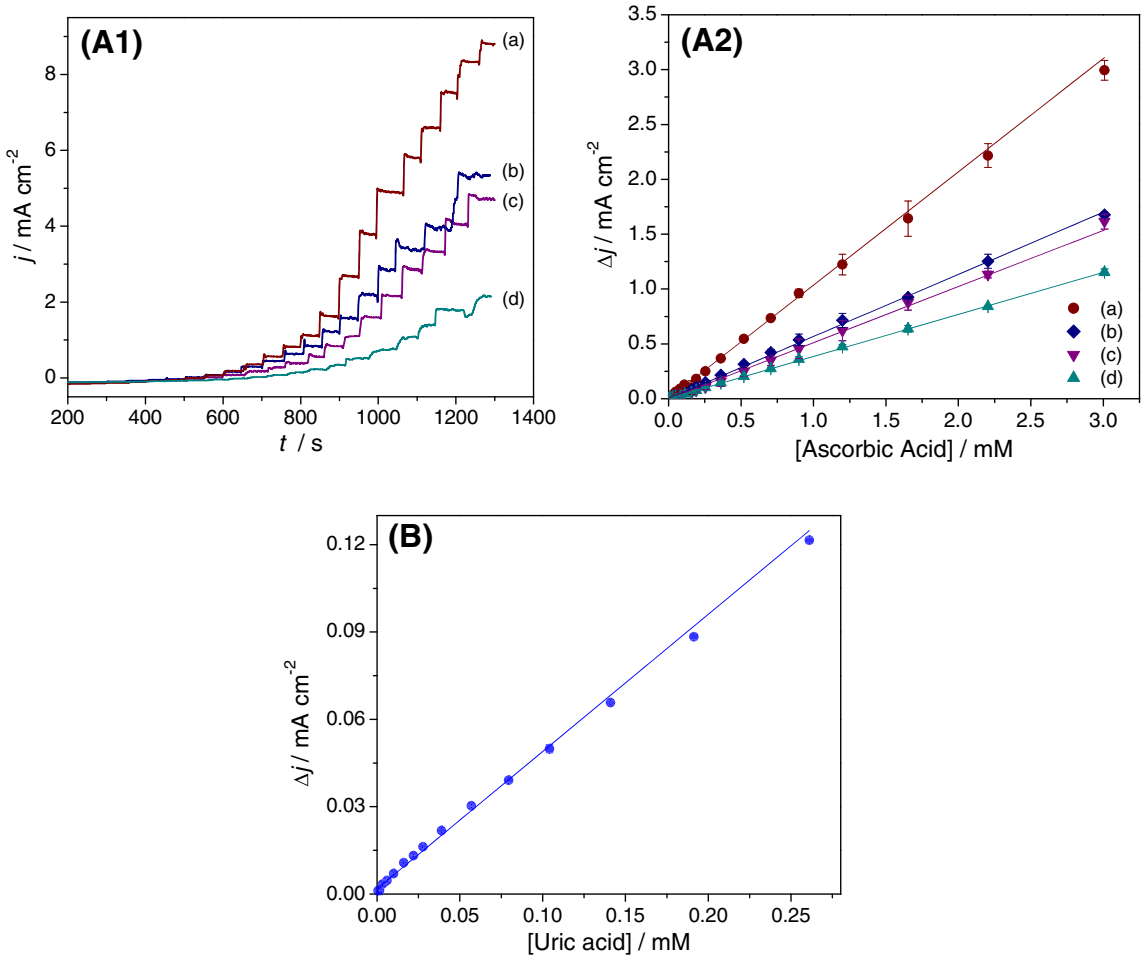

Fig. 6 (A1) Chronoamperometric response to AA at (a) $PTH_{DES}200$, (b) $PTH_{DES}100$, (c) $PTH_{DES}150$ and (d) $PTH_{DES}300$, on successive additions of AA in 0.1 M PB solution, pH = 7.0, applied potential 0.0 V vs. Ag/AgCl. (A2) Corresponding calibration plots. (B) Calibration plot of UOx/$PTH_{Ethaline}200$-CH_3COOH/MWCNT/GCE to UA in 0.1 M PB solution, pH = 7.0, applied potential + 0.30 V vs. Ag/AgCl. Error bars represent the standard deviation of three measurements and are too small to be visible in (B)

linear range 100–1000 μM. Biosensors with ascorbate oxidase enzyme, in one case immobilized on a screen-printed electrode by crosslinking with poly(ethylene glycol) diglycidyl ether had a LOD of 3 μM and range 5–150 μM [36], in the other case with gold nanoparticles and reduced graphene oxide on a GCE, had a detection limit of 17 μM and linear range 1000–5000 μM [37]. Finally, a graphene-modified BSA (G-BSA)–based sensor had a LOD of 25 μM and a range of 50–3000 μM [38].

Uric acid

Future biosensor applications were illustrated by using $PTH_{Ethaline}200$-CH_3COOH/MWCNT/GCE for constructing a uric acid biosensor, by immobilization of uricase (UOx), following the protocol described in the "Biosensor preparation" section. Results are displayed in Fig. 6B.

CV curves of the enzyme biosensor in 0.1 M PB in the absence and presence of the UA showed a maximum peak current of UA at + 0.30 V; this value of applied potential was chosen for fixed potential amperometry. The UOx/$PTH_{Ethaline}200$-CH_3COOH/MWCNT/GCE response to UA was linear between 0.48 and 279 μM with a sensitivity of 450 μA cm^{-2} mM^{-1} (3.53 μA mM^{-1}) and a LOD of 58.9 nM. The biosensor responded rapidly to changes in UA concentration, reaching 95% of the steady-state current in less than 7 s.

It showed excellent analytical performance, with fast response, good sensitivity, a wide linear working range and low detection limit compared with the literature from the last 5 years (Table 1). The detection limit of the new UOx/$PTH_{Ethaline}200$-CH_3COOH/MWCNT/GCE biosensor is very low compared with other reported uric acid sensors and biosensors [13, 22, 39–50]. There are two literature reports with higher sensitivity [45, 50]; however, the working potential for

detection are more positive than in our study [50] or the fabrication of a bioelectrode, that is more complicated [45]. A uric acid biosensor prepared by TH polymerization on MWCNT/GCE in aqueous media [22] gave a linear range of 2–100 μM and sensitivity of 182 μA cm^{-2} mM^{-1} for UA, and LOD of 0.8 μM. The $PTH_{Ethaline}$200-CH_3COOH/MWCNT/GCE in this work shows higher sensitivity, lower detection limit and wider working range.The repeatability and reproducibility of the UOx/$PTH_{Ethaline}$200-CH_3COOH/MWCNT/GCE were examined. The repeatability of the biosensor was investigated by plotting five successive calibration curves with the same electrode, and a relative standard deviation (RSD) was calculated using the slopes of these calibration curves. The RSD value was found as 3.5% at UOx/$PTH_{Ethaline}$200-CH_3COOH/MWCNT/GCE towards UA, which showed the high repeatability of the proposed sensor. The reproducibility was studied by five different modified electrodes the same way. The RSD was 5.4%, indicating that the fabrication of the biosensor was very reproducible. The operational stability was also investigated by measurement of the biosensor response to 0.2 mM UA. The RDS value was found to be 10.8% for UA after 30 consecutive measurements; the biosensor showed good operational stability.

The effect of common interfering species on the UOx/$PTH_{Ethaline}$200-CH_3COOH/MWCNT/GCE response was examined. The amperometric response of the biosensor to successive additions of 0.2 mM UA, 0.1 mM AA, 0.1 mM dopamine, 1.0 mM urea and 1.0 mM glucose in 0.1 M pH 7.0 PB was studied [11, 12]. Compared with UA response current, no significant effect on the biosensor response was observed in the presence of AA and dopamine interference species (less than 10%). Even at high concentrations of glucose and urea, the interaction effect can be neglected.

Application of the biosensor to synthetic urine

The performance of the UOx/$PTH_{Ethaline}$200-CH_3COOH/MWCNT/GCE biosensor was evaluated using synthetic urine spiked with known concentrations of UA. The synthetic urine was prepared according to the protocol in the "Reagents and solutions" section. A volume of 15 μL was added to the electrochemical cell containing 5 mL of PB buffer solution, and the final concentration of UA in the cell was 25.0 μM. The standard addition method was used to determine UA content in the synthetic urine sample with successive additions of 10 μL, 15 μL, 20 μL, 30 μL and 45 μL of 0.01 M standard UA solution to each spiked urine sample. The concentration of UA in spiked synthetic urine was calculated from this calibration curve. The UA concentration in the sample was found to be 25.2 ± 0.35 μM ($n = 3$) with UOx/$PTH_{Ethaline}$200-

Table 1 Comparison of analytical performances of amperometric sensors and biosensors with uricase, UOx, for the determination of UA

Modified electrode	Applied potential / V vs. Ag/AgCl	Linear range / μM	Sensitivity / μA cm^{-2} mM^{-1}	LOD / nM	Ref.
UOx/PBG/CNT/CFE	0.30 (SCE)	2–100	248	600	[22]
UOx/PTH/CNT/CFE			182	800	
UOx/Chi–CNTNF/AgNP/Au	− 0.35	1–400	–	1000	[39]
Nafion/UOx/ZnONS/Ag/Si	0.40	50–2000	129.81	19	[40]
UOx/GO/GCE	0.47	20–490	–	3450	[13]
PU/PL-A/UOx	0.65	100–700	0.8 nA μM^{-1}	< 10^3	* [41]
UOx/CuO/ZnO/ITO/glass bioelectrode	0.03	50–1000	870	5450	[42]
UOx/Pty/Pt/GCE	0.60	100–2500	0.943	10^3	[43]
UOx/poly(4-aminosalicylic acid)/PB/graphite SPE	− 0.10	10–200	–	3000	[44]
CeO_{2-x}/C/rGO	− 0.40 (SCE)	49.8–1050.0	284.5	2000	[45]
UOx/ZnO QD/Nafion	0.60	1000−1 × 10^4	4.0	22.97 × 10^3	[46]
Ta/Ni microcavity array film	0.45	1–1400	886	100	[47]
UOx/BLG-MWCNT-PtNP/GCE	0.40	20–500	31.131 μA μM^{-1}	800	* [48]
Cu_2O/Cu@C core-shell NW	− 0.50 (SCE)	50–1100	330.5	400	[49]
UOx/CH-Gr cry/PB/SPCE	0.0 (silver pseudo)	2.5–400	–	2500	[50]
UOx/$PTH_{Ethaline}$-CH_3COOH/MWCNT/GCE	0.30	0.48–279	450	58.9	This work

*Electrode area not stated. *PBG*, poly(brilliant green); *CFE*, carbon film electrode; *Chi–CNTNF*, chitosan-carbon nanotubes nanofiber; *AgNP*, silver nanoparticles; *ZnONS*, ZnO nanosheets; *GO*, graphene oxide; *PU*, urethane; *PL-A*, polyluminol:polyaniline; *ITO*, indium-tin oxide; *Pty*, polytyramine; *PB*, Prussian blue; *SPE*, screen-printed electrode; *rGO*, reduced graphene oxide; *QD*, quantum dots; *BLG*, β-lactoglobulin; *PtNP*, platinum nanoparticles; *NW*, nanowires; *CH-Gr*, chitosan graphene composite; *cry*, porous cryogel; *SPCE*, screen-printed carbon electrode

CH_3COOH/MWCNT/GCE biosensor. The mean recoveries ranged between 99.5 and 102.3%, with an average recovery of 100.8 ± 1.4%. From these results, it is concluded that the biosensor can be used to determine UA in urine samples with a good recovery.

Conclusions

The polymerization of TH on MWCNT/GCE in ethaline DES containing acetic acid dopant has been successfully carried out for the first time. The use of ethaline, an alternative "green designer solvent", in PTH synthesis has shown to be useful in the preparation of polymer films with different morphology. The scan rate, which is one of the electropolymerization parameters, also plays an important role in the PTH growth process and influences the electrochemical properties and performance of $PTH_{Ethaline}$-CH_3COOH/MWCNT/GCE. The PTH film prepared at 200 mV s^{-1} exhibited more uniform and smooth morphology and better electrochemical behaviour than with the other scan rates. As a result of the interaction between MWCNT and PTH polymer, the modified electrodes show better electrochemical performance because the structures of the composite materials have different physical and chemical properties.

The MWCNT/GCE modified with PTH was applied for AA sensing, that modified with $PTH_{Ethaline}$ films at 200 mV s^{-1} in ethaline DES presented the best sensing performance. UOx enzyme was immobilized on MWCNT/GCE modified with $PTH_{Ethaline}$ electrodeposited at 200 mV s^{-1} and successfully used for the monitoring of the uric acid with excellent analytical performance, and better than PTH films synthesized in aqueous solution in the literature. This $PTH_{Ethaline}$-CH_3COOH/MWCNT/GCE is a promising approach for uric acid and ascorbic acid analysis in real samples due to their high sensitivity, rapid response, easy fabrication and low cost.

Acknowledgements B. Dalkiran thankfully acknowledges the Scientific and Technological Research Council of Turkey (TUBITAK 2219) for a postdoctoral fellowship.

Funding The authors thank Fundação para a Ciência e a Tecnologia (FCT), Portugal, project PTDC/QEQ-QAN/2201/2014, in the framework of Project 3599-PPCDT, co-financed by the European Community Fund FEDER, and CEMMPRE, project UIDB/EMS/00285/2020 by FEDER funds through the program COMPETE – Programa Operacional Factores de Competitividade, and by national funds through FCT.

Compliance with ethical standards

Conflict of interest The authors declare that they have no conflicts of interest.

References

1. Valdés MG, González ACV, Calzón JAG, Díaz-García ME (2009) Analytical nanotechnology for food analysis. Microchim Acta 166: 1–19
2. Maduraiveeran G, Sasidharan M, Ganesan V (2018) Electrochemical sensor and biosensor platforms based on advanced nanomaterials for biological and biomedical applications. Biosens Bioelectron 103:113–129
3. Ben Messaoud N, Ghica ME, Dridi C, Ben Ali M, Brett CMA (2018) Electrochemical sensor based on multiwalled carbon nanotube and gold nanoparticle modified electrode for the sensitive detection of Bisphenol A. Sensors Actuators B Chem 255:2800–2808
4. Huang H, Yue Y, Chen Z, Chen Y, Wu S, Liao J, Liu S, Wen HR (2019) Electrochemical sensor based on a nanocomposite prepared from $TmPO_4$ and graphene oxide for simultaneous voltammetric detection of ascorbic acid, dopamine and uric acid. Microchim Acta 186:189
5. Barsan MM, Ghica ME, Brett CMA (2015) Electrochemical sensors and biosensors based on redox polymer/carbon nanotube modified electrodes: a review. Anal Chim Acta 881:1–23
6. Luong JH, Glennon JD, Gedanken A, Vashist SK (2017) Achievement and assessment of direct electron transfer of glucose oxidase in electrochemical biosensing using carbon nanotubes, graphene, and their nanocomposites. Microchim Acta 184:369–388
7. Tomé LIN, Baião V, da Silva W, Brett CMA (2018) Deep eutectic solvents for the production and application of new materials. Appl Mater Today 10:30–50
8. Hosu O, Barsan MM, Cristea C, Săndulescu R, Brett CMA (2017) Nanocomposites based on carbon nanotubes and redox-active polymers synthesized in a deep eutectic solvent as a new electrochemical sensing platform. Microchim Acta 184:3919–3927
9. Savi LK, Carpine D, Waszczynskyj N, Ribani RH, Haminiuk CWI (2019) Influence of temperature, water content and type of organic acid on the formation, stability and properties of functional natural deep eutectic solvents. Fluid Phase Equilib 488:40–47
10. Prathish KP, Carvalho R, Brett CMA (2016) Electrochemical characterisation of poly(3,4-ethylenedioxythiophene) film modified glassy carbon electrodes prepared in deep eutectic solvents for simultaneous sensing of biomarkers. Electrochim Acta 187:704–713
11. Xiao L, Chen J, Cha CS (2000) Elimination of the interference of ascorbic acid in the amperometric detection of biomolecules in body fluid samples and the simple detection of uric acid in human serum and urine by using the powder microelectrode technique. J Electroanal Chem 495(1):27–35
12. Yang L, Liu D, Huang J, You T (2014) Simultaneous determination of dopamine, ascorbic acid and uric acid at electrochemically reduced graphene oxide modified electrode. Sensors Actuators B Chem 193:166–172
13. Omar MN, Salleh AB, Lim HN, Tajudin AA (2016) Electrochemical detection of uric acid via uricase-immobilized graphene oxide. Anal Biochem 509:135–141
14. Ivanov A, Davletshina R, Sharafieva I, Evtugyn G (2019) Electrochemical biosensor based on polyelectrolyte complexes for the determination of reversible inhibitors of acetylcholinesterase. Talanta 194:723–730
15. da Silva W, Ghica ME, Brett CMA (2019) Novel nanocomposite film modified electrode based on poly (brilliant cresyl blue)-deep eutectic solvent/carbon nanotubes and its biosensing applications. Electrochim Acta 317:766–777
16. Carriazo D, Serrano MC, Gutiérrez MC, Ferrer ML, del Monte F (2012) Deep-eutectic solvents playing multiple roles in the synthesis of polymers and related materials. Chem Soc Rev 41:4996–5014

17. Zhang G, Zhang A, Liu X, Zhao S, Zhang J, Lu J (2010) Investigation of the electropolymerisation of o-toluidine and p-phenylenediamine and their electrocopolymerisation by in situ ultraviolet–visible spectroelectrochemistry. J Appl Polym Sci 115:2635–2647
18. Hosu O, Barsan MM, Cristea C, Săndulescu R, Brett CMA (2017) Nanostructured electropolymerized poly(methylene blue) films from deep eutectic solvents. Optimization and characterization. Electrochim Acta 232:285–295
19. Topçu E, Alanyalıoğlu M (2014) Electrochemical formation of poly(thionine) thin films: the effect of amine group on the polymeric film formation of phenothiazine dyes. J Appl Polym Sci 131: 39686-1–39686-9
20. Xu Y, Zhang X, Wang Y, He P, Fang Y (2010) Enhancement of electrochemical capacitance of carbon nanotubes by polythionine modification. Chin J Chem 28:417–421
21. Ghica ME, Ferreira GM, Brett CMA (2015) Poly(thionine)-carbon nanotube modified carbon film electrodes and application to the simultaneous determination of acetaminophen and dipyrone. J Solid State Electrochem 19:2869–2881
22. Ghica ME, Brett CMA (2014) Poly(brilliant green) and poly(thionine) modified carbon nanotube coated carbon film electrodes for glucose and uric acid biosensors. Talanta 130:198–206
23. Jia H, An J, Guo X, Su C, Zhang L, Zhou H, Xie C (2015) Deep eutectic solvent-assisted growth of gold nanofoams and their excellent catalytic properties. J Mol Liq 212:763–766
24. Kanazawa KK, Gordon JG (1985) The oscillation frequency of a quartz resonator in contact with liquid. Anal Chim Acta 175:99–105
25. Tenan MA, Soares DM (1998) The quartz crystal microbalance: a tool for probing viscous/viscoelastic properties of thin films. Braz J Phys 28:405–412
26. Stanford Research Systems (2004) Quartz crystal microbalance theory and calibration The QCM oscillator. Technical Reports 408: 744–9040
27. Yang R, Ruan C, Dai W, Deng J, Kong J (1999) Electropolymerisation of thionine in neutral aqueous media and H_2O_2 biosensor based on poly(thionine). Electrochim Acta 44: 1585–1596
28. Yang M, Guo ML, Feng YL, Lei YM, Cao YJ, Zhu DB, Yu Y, Ding L (2018) Sensitive voltammetric detection of metronidazole based on three-dimensional graphene-like carbon architecture/polythionine modified glassy carbon electrode. J Electrochem Soc 165:B530–B535
29. Raoof JB, Ojani R, Baghayeri M (2013) Fabrication of layer-by-layer deposited films containing carbon nanotubes and poly(malachite green) as a sensor for simultaneous determination of ascorbic acid, epinephrine, and uric acid. Turk J Chem 37:36–50
30. Molina J, Del Río AI, Bonastre J, Cases F (2010) Influence of the scan rate on the morphology of polyaniline grown on conducting fabrics, centipede-like morphology. Synth Met 160:99–107
31. Kellenberger A, Ambros D, Plesu N (2014) Scan rate dependent morphology of polyaniline films electrochemically deposited on nickel. Int J Electrochem Sci 9:6821–6833
32. Han D, Han T, Shan C, Ivaska A, Niu L (2010) Simultaneous determination of ascorbic acid, dopamine and uric acid with chitosan- graphene modified electrode. Electroanal 22:2001–2008
33. Habibi B, Pournaghi-Azar MH (2010) Simultaneous determination of ascorbic acid, dopamine and uric acid by use of a MWCNT modified carbon-ceramic electrode and differential pulse voltammetry. Electrochim Acta 55:5492–5498
34. Sheng ZH, Zheng XQ, Xu JY, Bao WJ, Wang FB, Xia XH (2012) Electrochemical sensor based on nitrogen doped graphene: simultaneous determination of ascorbic acid, dopamine and uric acid. Biosens Bioelectron 34:125–131
35. Luo J, Jiang S, Liu R, Zhang Y, Liu X (2013) Synthesis of water dispersible polyaniline/poly(styrenesulfonic acid) modified graphene composite and its electrochemical properties. Electrochim Acta 96:103–109
36. Csiffáry G, Fűtő P, Adányi N, Kiss A (2016) Ascorbate oxidase-based amperometric biosensor for L-ascorbic acid determination in beverages. Food Technol Biotechnol 54:31–35
37. Ma J, Xu J, Yang C, Song J, Fu Y (2018) An ascorbic acid oxidase-based sensing platform for stereoselective interaction with ascorbic acid and isoascorbic acid. Anal Sci 34:427–432
38. Askari E, Naghib SM (2018) Novel approach to facile synthesis and biosensing of the protein-regulated graphene. Int J Electrochem Sci 13:886–897
39. Numnuam A, Thavarungkul P, Kanatharana P (2014) An amperometric uric acid biosensor based on chitosan-carbon nanotubes electrospun nanofiber on silver nanoparticles. Anal Bioanal Chem 406:3763–3772
40. Ahmad R, Tripathy N, Jang NK, Khang G, Hahn YB (2015) Fabrication of highly sensitive uric acid biosensor based on directly grown ZnO nanosheets on electrode surface. Sensors Actuators B Chem 206:146–151
41. Conway GE, Lambertson RH, Schwarzmann MA, Pannell MJ, Kerins HW, Rubenstein KJ, Leopold MC (2016) Layer-by-layer design and optimization of xerogel-based amperometric first generation biosensors for uric acid. J Electroanal Chem 775:135–145
42. Jindal K, Tomar M, Gupta V (2017) A novel low-powered uric acid biosensor based on arrayed pn junction heterostructures of ZnO thin film and CuO microclusters. Sensors Actuators B Chem 253:566–575
43. Situmorang M, Nurwahyuni I (2017) The development of reproducible and selective uric acid biosensor by using electrodeposited polytyramine as matrix polymer. Indo J Chem 17:461–470
44. da Cruz FS, Paula FS, Franco DL, dos Santos WTP, Ferreira LF (2017) Electrochemical detection of uric acid using graphite screen-printed electrodes modified with Prussian blue/poly(4-aminosalicylic acid)/uricase. J Electroanal Chem 806:172–179
45. Peng B, Cui J, Wang Y, Liu J, Zheng H, Jin L, Wu Y (2018) CeO_2−x/C/rGO nanocomposites derived from Ce-MOF and graphene oxide as a robust platform for highly sensitive uric acid detection. Nanoscale 10:1939–1945
46. Ali M, Shah I, Kim SW, Sajid M, Lim JH, Choi KH (2018) Quantitative detection of uric acid through ZnO quantum dots based highly sensitive electrochemical biosensor. Sensors Actuators A Phys 283:282–290
47. Zhao M, Zhao J, Qin L, Jia H, Liu S (2019) Synthesis of Ta/Ni microcavity array film for highly sensitive uric acid detection. J Electroanal Chem 834:86–93
48. Han B, Pan M, Liu X, Liu J, Cui T, Chen Q (2019) Electrochemical detection for uric acid based on β-lactoglobulin-functionalized multiwall carbon nanotubes synthesis with PtNPs nanocomposite. Materials 12:214
49. Luo J, Cui J, Wang Y, Yu D, Qin Y, Zheng H, Wu Y (2020) Metal-organic framework-derived porous Cu_2O/Cu@C core-shell nanowires and their application in uric acid biosensor. Appl Surf Sci 506:144662
50. Jirakunakorn R, Khumngern S, Choosang J, Thavarungkul P, Kanatharana P, Numnuam A (2020) Uric acid enzyme biosensor based on a screen-printed electrode coated with Prussian blue and modified with chitosan-graphene composite cryogel. Microchem J 154:104624

Publisher's note Springer Nature remains neutral with regard to jurisdictional claims in published maps and institutional affiliations.